

SPEAR-1, AN EXPERIMENT TO MEASURE CURRENT COLLECTION IN THE
IONOSPHERE BY HIGH VOLTAGE BIASED CONDUCTORS

W. John Raitt, Neil B. Myers, Jon A. Roberts, and D. C. Thompson

Center for Atmospheric and Space Science, Utah State University,
Logan, Utah 84322-4405

Abstract. An experiment will be described in which a high electrical potential difference, up to 45 kV, was applied between deployed conducting spheres and a sounding rocket in the ionosphere. Measurements were made of the applied voltage and the resulting currents for each of 24 applications of different high potentials. In addition, diagnostic measurements of optical emissions in the vicinity of the spheres, energetic particle flow to the sounding rocket, DC electric field and wave data were made. The ambient plasma and neutral environments were measured by a Langmuir probe and a cold cathode neutral ionization gauge, respectively.

In this presentation, the payload will be described and examples of the measured current and voltage characteristics will be presented. The characteristics of the measured currents will be discussed in terms of the diagnostic measurements and the in-situ measurements of the vehicle environment.

In general, it was found that the currents observed were at a level typical of magnetically limited currents from the ionospheric plasma for potentials less than 12 kV, and slightly higher for larger potentials. However, due to the failure to expose the plasma contactor, the vehicle sheath modified the sphere sheaths and made comparisons with the analytic models of Langmuir-Blodgett and Parker-Murphy less meaningful. Examples of localized enhancements of ambient gas density resulting from the operation of the attitude control system thrusters (cold nitrogen) were obtained. Current measurements and optical data indicated localized discharges due to enhanced gas density reduced the vehicle-ionosphere impedance.

Background

A vehicle in space will attain an electrical potential with respect to the background environment in order to balance the ion and electron fluxes to the vehicle which differ greatly when the vehicle is at the background plasma potential. The causes for the difference in fluxes may include the larger thermal velocity of electrons compared to ions, secondary electron emission from the vehicle due to ion impact, photoemission of electrons due to sunlight, and any active emission of either electrons or ions. Much of the literature has been concerned with environmentally induced charging of geosynchronous satellites which can attain potentials of tens of kilovolts with respect to the background plasma. Recently, interest in the charging of vehicles in the lower ionosphere has increased because of the planned use of large space vehicles with high power requirements (such as the space station) at low Earth orbit (LEO) altitudes. Numerous electron beam experiments have been performed in the lower ionosphere to study the processes that occur when exposing high potentials to the space environment [Winckler, 1980; Szuszczewicz, 1985]. It was found that electron beam emission

complicated the interpretation of these processes and could change the current collection characteristics of the beam-emitting vehicle [Myers et al., GRL, 1989].

The Space Power Experiments Aboard Rockets (SPEAR) program was initiated to provide guidelines in designing high voltage (HV) systems that utilize the near vacuum of the space environment as insulation at LEO altitudes. The development of these guidelines requires better understanding of the physics of the HV interaction with LEO environment. The SPEAR program has involved a theoretical modelling group, a ground-based laboratory group, and a flight experiments group to study HV interaction with plasmas.

Science Objectives

The science objectives of the SPEAR-1 experiment were to; 1) study the altitude dependence of the current-voltage characteristics of a metallic conductor exposed to the space environment when biased up to tens of kilovolts, 2) study the interaction of high voltage biased conductors within each other's charge sheaths, 3) make diagnostic measurements to aid the development of theoretical models to predict the current collection by conductors biased to high voltages in the ionosphere, 4) study the effectiveness of a plasma contactor in grounding the power platform to the ambient ionosphere, and 5) obtain this data in a timely fashion to be useful in the SPEAR-2 program.

Principle of Experiment

The SPEAR-1 experiment included two spherical conductors separated from the upper portion of the rocket body by a fiberglass boom and biased to potentials as large as 45 kV. Spherical conductors were employed to enable a comparison of current collection from a space plasma with analytic models [Langmuir and Blodgett, 1924; Parker and Murphy, 1967; and Linson, 1969]. The upper portion of the boom utilized a grading ring structure to ensure a uniform potential drop from the spheres to the main portion of the boom that was maintained at the rocket body potential. The grading rings also reduce the possibility of surface flashover on the boom by hiding triple points from the ambient ionospheric plasma. A plasma contactor was located on the lower portion of the rocket body to clamp the main vehicle potential near the plasma potential. The potential between the rocket and the spheres was measured and the current collected by the spheres was determined. A low light level television (LLTV) camera and three photometers were used to measure light emission accompanying the current collection of the spheres. Figure 1 shows the general configuration of the payload and the location of the instruments. A series of bias operations was performed to study the altitude dependence of the HV interaction. An attitude control system (ACS) stabilized the rocket body with the spheres in three different orientations relative to the geomagnetic field, allowing magnetic effects of the HV interaction to be studied.

Payload Arrangement

The two spheres were made from aluminum plated with gold over nickel. The diameter of the spheres was 0.2 m. The grading rings were

shallow, saucer shaped rings made of aluminum with nickel plating. The grading rings were separated by resistors between adjacent rings. The rings were oriented to prevent electrons accelerated to the spheres from striking the boom. The total resistance of the grading rings to sphere 1 was 1.1 M Ω , and to sphere 2 was 980 k Ω . The difference was due to the slightly different lengths of the two grading ring booms necessary to accommodate the spheres and booms in their folded, pre-deployment configuration.

A LLLTV camera with a wide angle lens was located to view both spheres and their charge sheaths to an area extending about 5 m from either side of the spheres. One of the guiding rods for nosecone deployment blocked the view of sphere 2 during most of the flight although portions of the charge sheath were not obstructed. Figure 2 shows the location of the LLLTV (and some of the other instruments) with respect to the spheres.

Three photometers were oriented to view the region between the spheres with a field-of-view of 5° half-maximum full-width. The photometers measured wavelengths of 476.5 nm, 441.5 nm, and 391.4 nm, which correspond to emissions from Ar⁺, O⁺, and N₂⁺ respectively. Ar⁺ was chosen because the plasma contactor released argon gas.

A cold cathode ionization gauge provided measurements of neutral pressure in the range of 10⁻³ to 10⁻⁷ torr. The neutral pressure gauge was located in the upper portion of the rocket, placing it as far as possible from the plasma contactor, and as close as possible to the HV spheres.

The high voltages were applied to the spheres using 2.5- μ F capacitors charged to voltages between 6 kV and 45 kV. Different potentials were applied to the two spheres, and at times a potential was applied to only sphere 1. Fixed resistors were connected to the capacitors in parallel to the rocket ground to ensure that the capacitors completely discharged within about five seconds. The equivalent circuit diagram for sphere 1 is shown in Figure 3. All of the known resistances were the same for sphere 2 except that of the grading ring resistance.

A cylindrical Langmuir probe was deployed radially from the rocket body with a total collection area of about 0.001 m² to measure the ambient plasma density. The probe voltage was swept from +5 V to -1 V and back again over a period of one second, which repeated every 2.3 seconds.

Electrostatic waves were measured by two single-axis antennas deployed radially 1 m from the rocket. Very low frequency (VLF) waves were monitored from 20 Hz to 30 kHz with varying bandwidths up to 20 kHz. High frequency (HF) waves were measured with a 200-kHz bandwidth up to 10 MHz.

Four imaging ion and electron detectors monitored particle fluxes in the energy ranges of 2 eV to 5 keV and 10 eV to 30 keV with several view directions and a 32 ms spectral resolution. The higher energy bandwidths were about 11% of the energy channel while the lower energy bandwidths were about 20%.

A hollow cathode plasma contactor was intended to clamp the vehicle potential to between -100 and -150 V during voltage bias operations. The plasma contactor was located at the bottom of the rocket body to minimize contamination of the sphere environment.

Flight Operations

SPEAR-1 was launched at 20:45 EST on December 13, 1987 from the NASA Wallops Flight Facility, Virginia. The vehicle reached an apogee of 369 km at 351 seconds mission elapsed time (MET). The ACS was used to place the spheres into three orientations with respect to the geomagnetic field as shown in Figure 4. The first orientation was such that the plane described by the v-shaped booms deploying the spheres was nearly perpendicular to the geomagnetic field. In the second orientation the plane of the v-shaped booms of the spheres was parallel to the geomagnetic field. In the third orientation the sphere 1 boom was parallel to the geomagnetic field. Twenty four voltage bias operations were performed between 192 seconds and 622 seconds as shown in Figure 5. The altitude of the rocket is shown versus MET. The bias operations are shown with the voltage bias of sphere 1 above the trajectory and that of sphere 2 below the trajectory. The three orientations of the spheres with respect to the geomagnetic field are also shown.

Measurements

Atmospheric Parameters

A comparison of the neutral pressure measured during the experiment with that predicted by the MSIS-86 model [Hedin, 1987] is shown in Figure 6. Pressure in torr is shown versus MET in seconds. The difference between the measurements and the model is attributed to outgassing from the instrument initially, and outgassing of the fiberglass boom (located very near the instrument) and the rocket body. Since the mean free path is large, we can assume that the pressure at the spheres due to outgassing decreased by the inverse square of the distance to the spheres. This yields pressures at the spheres in agreement with the MSIS model results.

The electron density derived from the Langmuir probe during the experiment is shown in Figure 7. Altitude is shown versus measured electron density (squares) and electron density predicted by the IRI model [Rawer et al., 1981] (triangles). The electrons in the ionosphere are more dynamic than the neutrals, and as a result the IRI model results are not in good agreement with the measurements. No density measurements were obtained during the discharges. The plasma density was measured to be lower during downleg, since the Langmuir probe was in the vehicle wake during the downleg portion of the flight. The electron temperature was also derived from the Langmuir probe data and is shown in Figure 8. Altitude is shown versus the measurement of temperature (squares) and the electron temperature prediction from the IRI model (triangles).

Current-Voltage

Raw Measurements. The currents measured directly during voltage bias operations were the current down the grading ring boom, $I(b)$, and the total current to the capacitor, $I(t)$, as seen in Figure 3. The plasma current to the sphere is obtained by subtracting $I(b)$ and the current through the 700 k Ω resistor from $I(t)$. The measurements of

$I(t)$ and $I(b)$ and the resulting derived plasma current are shown in Figure 9 for one of the voltage bias operations. The individual currents are shown versus increasing potential. The potential was the measured potential of the capacitor, which would equal the potential of the sphere with respect to the background ionosphere if the plasma contactor had been able to clamp the rocket body to the ionospheric potential. Unfortunately, the cover on the plasma contactor failed to deploy preventing the plasma contactor from being exposed to space. This allowed the rocket body to charge to several kilovolts negative during voltage bias operations. Time increased with decreasing potential since the bias operations applied the full potential to the spheres that subsequently decayed to zero voltage. There were no large current spikes in the measurements, indicating that no discharges occurred between the plasma and the spheres in space.

Numerous discharges were observed during pre-flight vacuum chamber tests. This can be seen in Figure 10, which shows $I(t)$, $I(b)$, and the potential on the sphere versus time during the vacuum chamber tests. The discharges can be seen as the large current spikes of $I(t)$ that resulted in the sharp decreases in the measured potential. The contrasting results demonstrate the difference between an experiment in a vacuum chamber and in space.

Plasma Currents. A series of voltage bias operations is shown in Figure 11. Plasma current is shown versus the capacitor potential for three different altitudes. The measurements for sphere 1 are shown on the left, and the measurements for sphere 2 are shown on the right. The sheath resistance has been calculated using the capacitor potential and the plasma current as shown in the figure, ranging from 900 k Ω to 5.9 M Ω . These calculations are larger than the actual sheath resistance since the actual sphere potential can be several kilovolts less than the capacitor potential. The data obtained at 257 km show three enhancements to current collected by the spheres. The LLLTV images showed brief bursts of light around the grading rings after the initial glow had disappeared. The presumed cause of the current enhancements was the outgassing of the grading rings since this was the first bias operation. An interesting curve of the $i-v$ characteristic is seen in the sphere 2 data obtained at 303 km (panel e). The sphere current increased as the potential decreased from 5 kV to near zero. This is thought to be due to the impingement of the rocket body ion sheath on the electron sheath of the sphere. Initially the potential on sphere 1 was 36 kV and the potential of the rocket body was several kilovolts negative. The rocket body must develop a very large ion sheath to attract ions from the plasma [Katz et al., 1989]. This large ion sheath would partially envelope the electron sheath of the spheres, decreasing the current collection by the spheres. As the potential on the capacitor decayed, the rocket body ion sheath decreased in size, reducing the interaction of the charge sheaths and allowing an increased current to the spheres.

The rocket body potential could be inferred at times from the particle detector data. Two sweeps of the particle detector data obtained at 361 km are shown in Figure 12. The data of the top panel show a peak at about 6 kV with a width from 4 to 9 kV. The rocket body potential is interpreted to be between 4 and 9 kV. The large number of lower energy electrons are due to ionization in the sheath. The data in the lower panel were obtained almost a second later and the rocket body potential has decreased to between 1 and 5 kV. The actual sphere

potential with respect to the ionosphere can be calculated using the rocket body potential measured during each sweep and is shown in Figure 13 for the data obtained at 361 km. There is a large uncertainty in the rocket body potential obtained in this fashion and not all of the particle detector sweeps were as simple to interpret as the ones shown in Figure 12, complicating the usefulness of this procedure.

Three bias operations that applied the maximum potential (45 kV) to sphere 1 exhibited a current enhancement at the largest potential on the sphere. An example of this is shown in Figure 13 for the data obtained at 361 km, which shows plasma current versus capacitor potential and the corresponding predictions of the Langmuir-Blodgett (dashed line) and Parker-Murphy (solid line) models. The LLLTV images showed a diffuse glow around the grading rings which moved toward the connection point of the two graded booms. This is possibly a volume discharge at potentials greater than 40 kV for the geometry of the experiment.

Since the electron density remained fairly constant over the altitude range of the voltage bias operations, no definite trend was seen in the calculated sheath resistance over the altitude range of the experiment. There was a dependence on the orientation of the spheres with respect to the geomagnetic field. The sheath resistances were between 100 k Ω and 250 k Ω lower in the V-plane parallel orientation compared to the V-plane perpendicular. This is about 15% of the total sheath resistance, however there were only three discharges for comparison in the parallel case.

Considerable ACS activity occurred during two voltage bias operations because of attitude changes of the rocket body just prior to the bias operations. The ACS thruster firings resulted in temporary enhancements to the current collected by the spheres. Figure 14 shows the capacitor voltage and plasma current versus time for a bias operation without ACS activity at 285 km (left) and with ACS activity at 235 km (right). The current enhancements are seen as the spikes in the plasma current (up to 0.15 A) in the lower right panel. The current enhancements had very little effect on the capacitor potential since the charge required to produce these spikes was small compared to the charge stored in the capacitor. Figure 15 shows the plasma current and ACS nozzle firings versus time for the operations at 352 km (top two panels) and at 235 km (lower two panels). There is a strong correlation between the ACS nozzle firings and the enhanced current spikes. The misalignments of some of the current spikes with the ACS nozzle firings can be explained by the slower sample rate of the ACS data.

The ACS operations from the rocket body may effectively neutralize the rocket body potential, functioning as a plasma contactor [B.E. Gilchrist et al., Observations of electron collection enhancement using neutral gas thruster jets on an isolated charged vehicle in the ionosphere, in press, *J. Geophys. Res.*, 1989; N.B. Myers et al., Vehicle charging effects during electron beam emission from the CHARGE-2 experiment, in press, *J. Space Rockets*, 1989]. Under these circumstances the rocket sheath impedance (Figure 3) becomes short circuited by the ionization in the thruster jet, thereby reducing the total series impedance in the capacitor discharge circuit. Thus, the capacitor potential may represent the sphere-to-ionosphere potential during the portions of the voltage bias operations with ACS firings, allowing a comparison of the current collection with analytic current-

voltage models. This has been done in Figure 16. The top panel shows the plasma current to the sphere during ACS firings versus potential compared with the Langmuir-Blodgett (dashed line) and the Parker-Murphy (solid line) models at 353 km. The middle panel shows the data obtained at 235 km with the same format. The lower panel shows the collected current during ACS firings normalized to the Parker-Murphy model for all cases of ACS firings during voltage operations. The data agree well with the Parker-Murphy model at potentials less than 12 kV. This is in agreement with the CHARGE-2 results for the current collection of a 1-kV conductor in the ionosphere [Myers et al., 1989]. Above 12 kV The collected current exceeds that of the Parker-Murphy model but is still substantially less than that of the Langmuir-Blodgett model.

Optical Data

LLTV. The view from the LLLTV camera is represented in Figure 17. The camera was located at the top of the payload looking forward at the deployed spheres. Three guiding rods for the nosecone deployment are in the field-of-view of the camera. One of the guiding rods partially obstructs sphere 2 and a portion of its grading ring boom. The wire that connects the HV capacitors with the spheres is visible connecting the main payload with the two grading ring booms. The time tag of the video is usually seen as a blur in the lower right corner of the reproduction of the single freeze-frame images.

A typical image during a voltage bias operation is shown in Figure 18. A 7-kV potential was applied to sphere 1 and a 21-kV potential was applied to sphere 2. A glow surrounding the spheres and extending down the grading ring booms is evident in the image, although the guiding rod partially obstructs the glow of sphere 2. The airglow layer is also seen in the image. The glow during voltage biasing was always seen around both the spheres and their guiding rods whenever it was visible. Relative intensity measurements from the digitized images show that the glow is about the same brightness as the airglow.

Figure 19 shows an image during the same voltage bias operation just after a vehicle maneuver and coincident with an ACS thruster firing from the rocket body. The thruster firing must have resulted in a localized generation of light caused by impact ionization of the released neutral gas by the charged particles accelerated by the rocket potential. The light generated in the thruster cloud can be seen reflected from two of the guiding rods, the main boom, and its wire. The light must have been fairly localized since a sharp shadow was produced on one side of the wire and can be seen where the wire crosses the main boom.

The image shown in Figure 20 indicates a possible volume discharge as evidenced by the large glow that can be seen at the connection point of the two grading ring booms. The airglow layer is seen extending partially through that region. A 43-kV potential was applied to sphere 1, while no potential was applied to sphere 2. This type of glow was only seen for the three single-sphere bias operations of bias voltages greater than 40 kV. The diffuse glow was seen in the video images to move along the grading rings toward the connection point of the booms.

Photometer. No correlation of light measurements with voltage bias operations was seen in any of the photometer channels. The field-of-view of the photometers was the region between the spheres, whereas the

largest light emission occurred in the volume surrounding the grading ring booms. All three photometers showed increased light measurements when the airglow layer passed through their field-of-view.

Summary and Conclusions

The SPEAR-1 payload successfully applied up to 45 kV to two spherical conductors in the ionosphere. Negligible volume discharge effects occurred when the HV interacted with the LEO environment, in the geometrical configuration used. The rocket body potential was probably near ambient plasma potential during ACS thruster firings. During those times it was determined that the sphere current collection was magnetically limited and in agreement with the Parker-Murphy model for potentials less than 12 kV. The collected current exceeded the Parker-Murphy model for potentials above 12 kV. The net space load placed on the power supply was well represented by a linear resistance of 500-1000 k Ω for the geometry of the SPEAR-1 payload. Negative potentials of up to 10 kV on the rocket body resulted in no adverse effects resulting from transient surface discharges. Transient discharge currents were triggered by release of neutral gas from the rocket body during voltage bias operations. The SPEAR-1 payload demonstrated the feasibility of using high energy, high voltage capacitors on a space vehicle.

Acknowledgements. The SPEAR-1 rocket flight was funded by the Defense Nuclear Agency under grant DNA001-87-C-0015.

References

- Hedin, A. E., MSIS-86 Thermospheric model, *J. Geophys. Res.*, 92, 4649, 1987.
- Langmuir, I. and K. Blodgett, Current limited by space charge flow between concentric spheres, *Phys. Rev.*, 24, 49, 1924.
- Linson, L. M., Current-voltage characteristics of an electron-emitting satellite in the ionosphere, *J. Geophys. Res.*, 74, 2368, 1969.
- Myers, N. B., W. J. Raitt, B. E. Gilchrist, P. M. Banks, T. Neubert, P. R. Williamson, and S. Sasaki, A comparison of current-voltage relationships of collectors in the Earth's ionosphere with and without electron beam emission, *Geophys. Res. Lett.*, 16, 365, 1989.
- Parker, L. W. and B. L. Murphy, Potential buildup on an electron-emitting ionospheric satellite, *J. Geophys. Res.*, 72, 1631, 1967.
- Rawer, K., S. Ramakrishnan, D. Bilitza, International reference ionosphere 1978, URSI Brussels and World Data Center, Report UAG-82, Boulder, 1981.
- Szuszczewicz, E. P., Controlled electron beam experiments in space and supporting laboratory experiments: a review, *Journal of Atmospheric and Terrestrial Physics*, 47, 1189, 1985.
- Winckler, J. R., The application of artificial electron beams to magnetospheric research, *Reviews of Geophysics and Space Physics*, 18, 659, 1980.

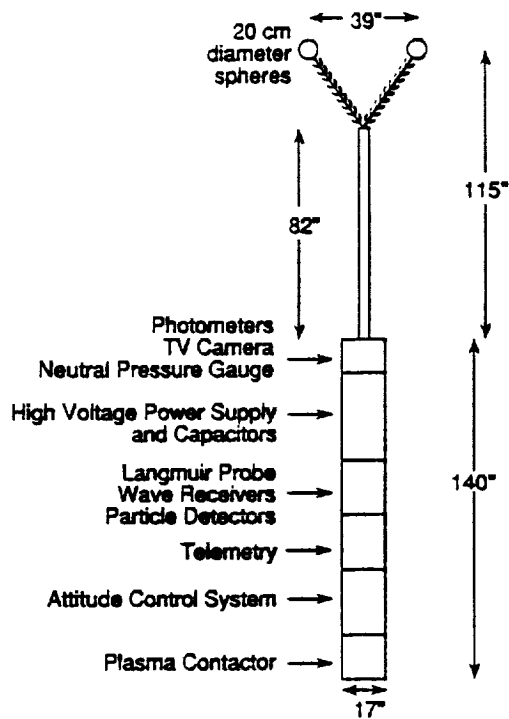


Fig. 1. Schematic diagram of the payload configuration of the SPEAR-1 experiment.

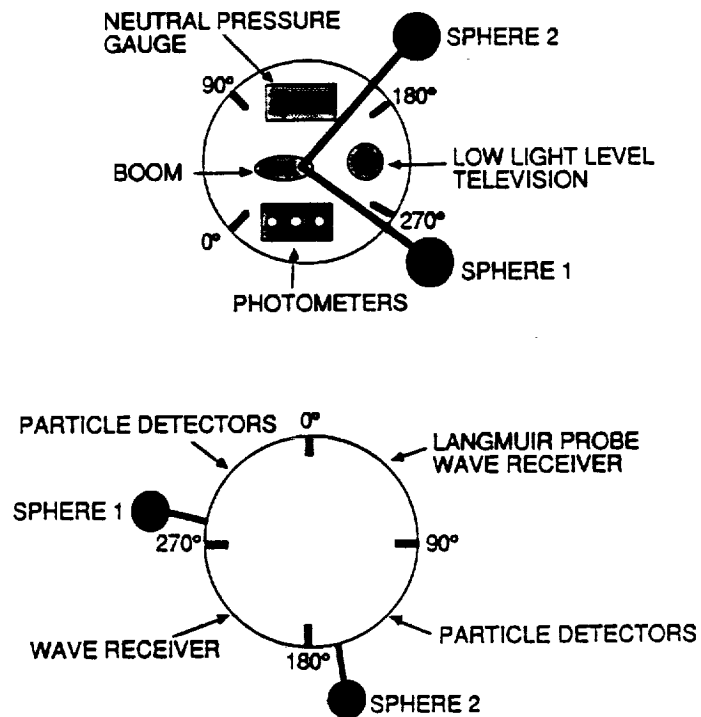


Fig. 2. Schematic diagram of the cross-section of the SPEAR-1 payload. Top panel shows view from the top of the rocket while the lower panel shows the view from the bottom of the rocket.

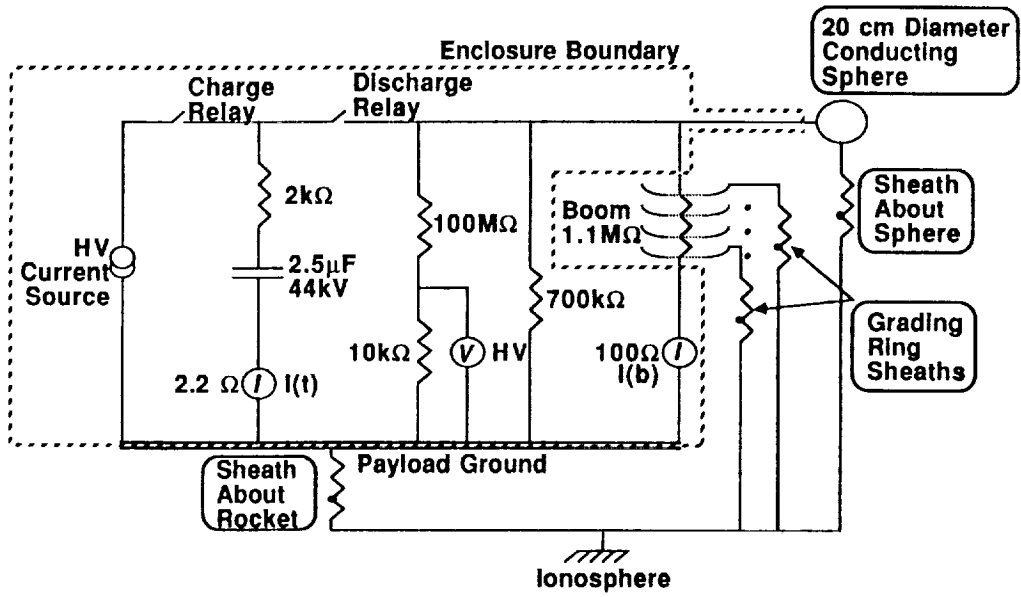
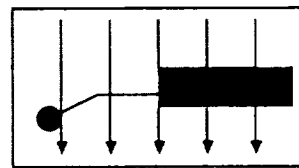
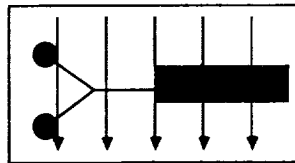


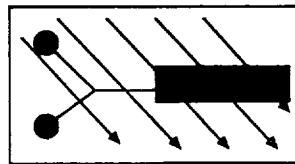
Fig. 3. Equivalent electrical circuit diagram for sphere 1.



V-PLANE PERPENDICULAR



V-PLANE PARALLEL



SPHERE 1 BOOM PARALLEL

Fig. 4. Schematic representation of the three vehicle orientations with respect to the Earth's magnetic field represented by arrows.

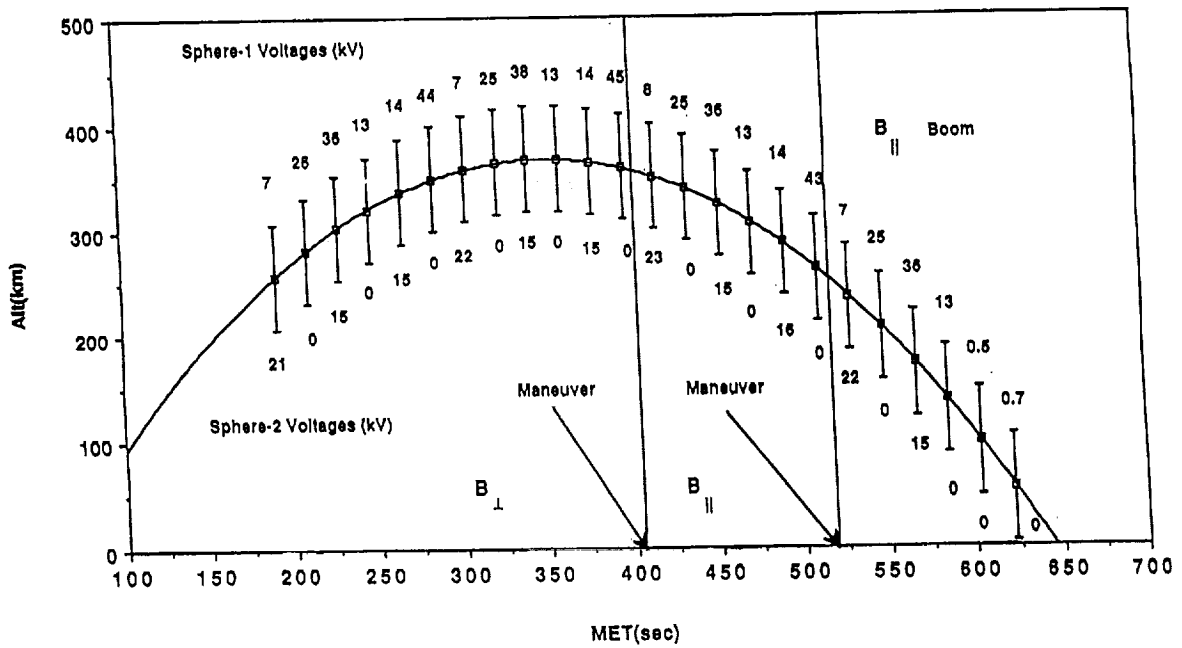


Fig. 5. Trajectory of the SPEAR-1 payload with the voltage bias operations included. The maximum potentials are given for sphere 1 (above the trajectory) and sphere 2 (below the trajectory). The two maneuvers accomplished by the ACS to achieve the three orientations are also shown.

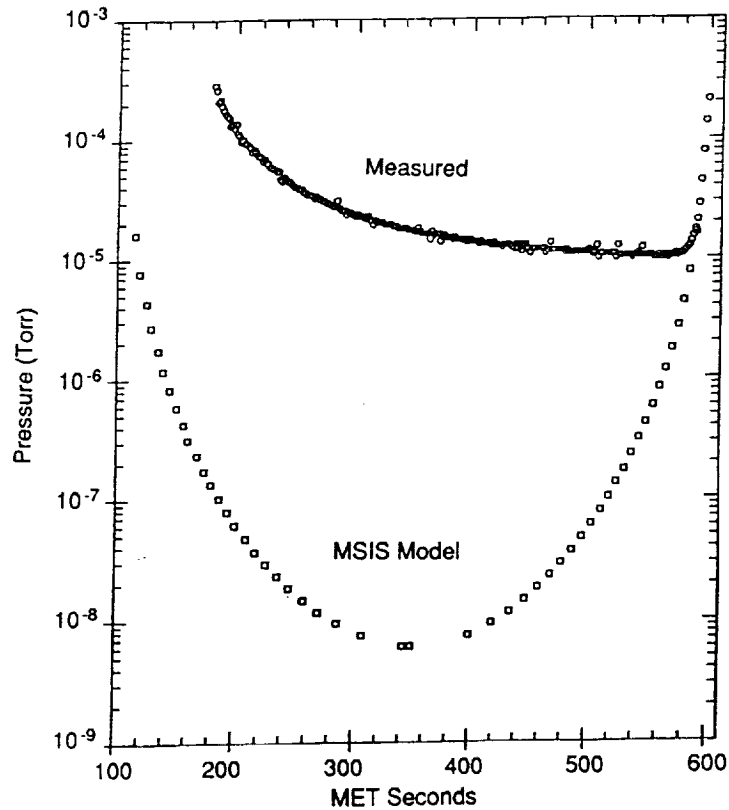


Fig. 6. Comparison of the neutral pressure measured during the experiment and calculated using the MSIS-86 model.

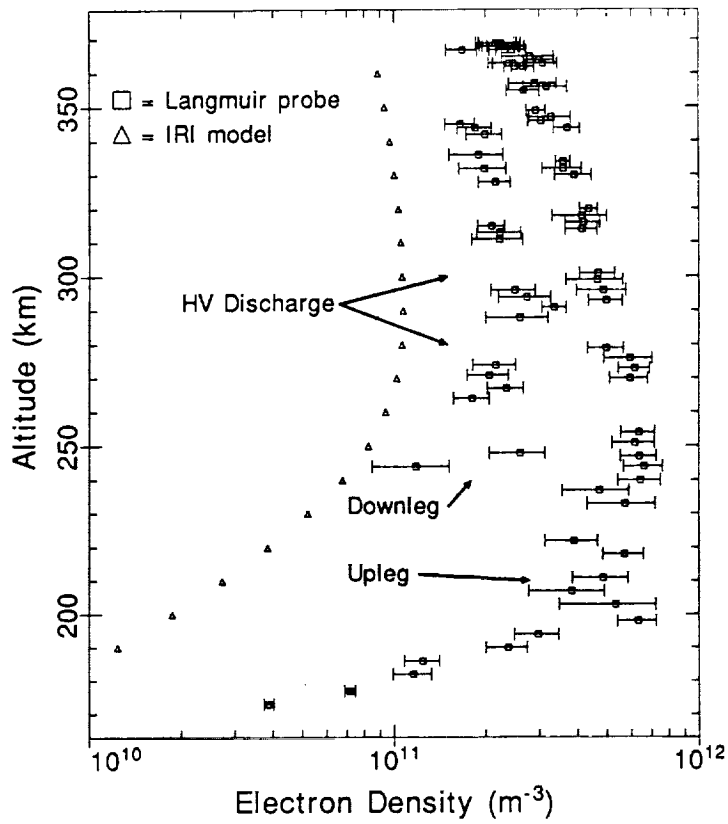


Fig. 7. Comparison of the electron density measured during the experiment and calculated using the IRI model.

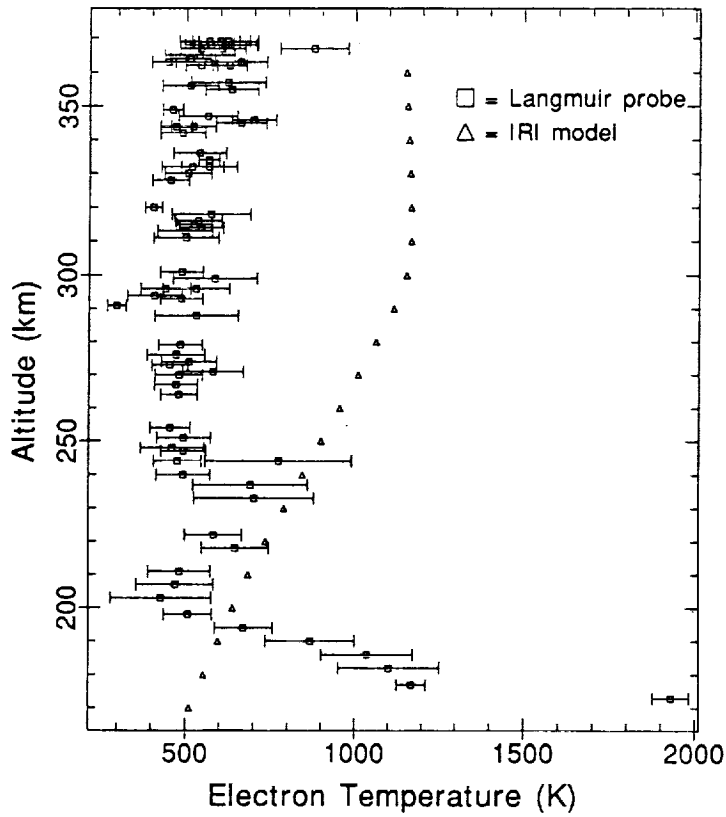


Fig. 8. Comparison of the electron temperature measured during the experiment and calculated using the IRI model.

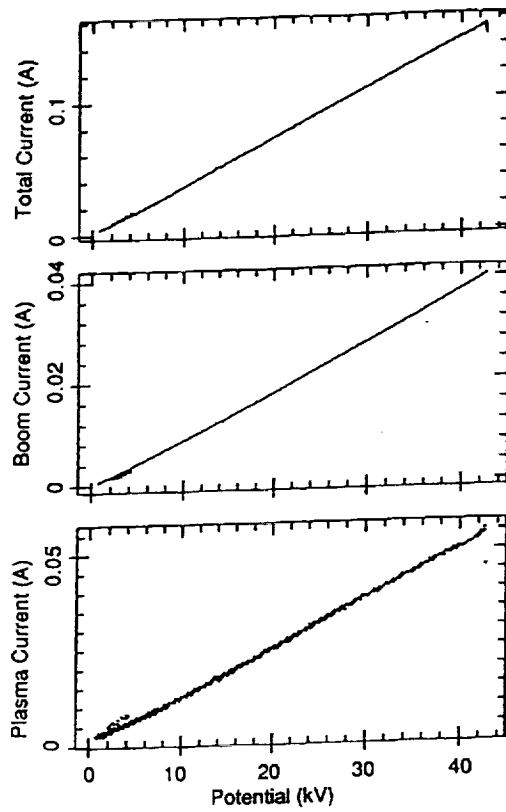


Fig. 9. The measured boom and total current, and the derived plasma current to the sphere versus the potential applied to sphere 1.

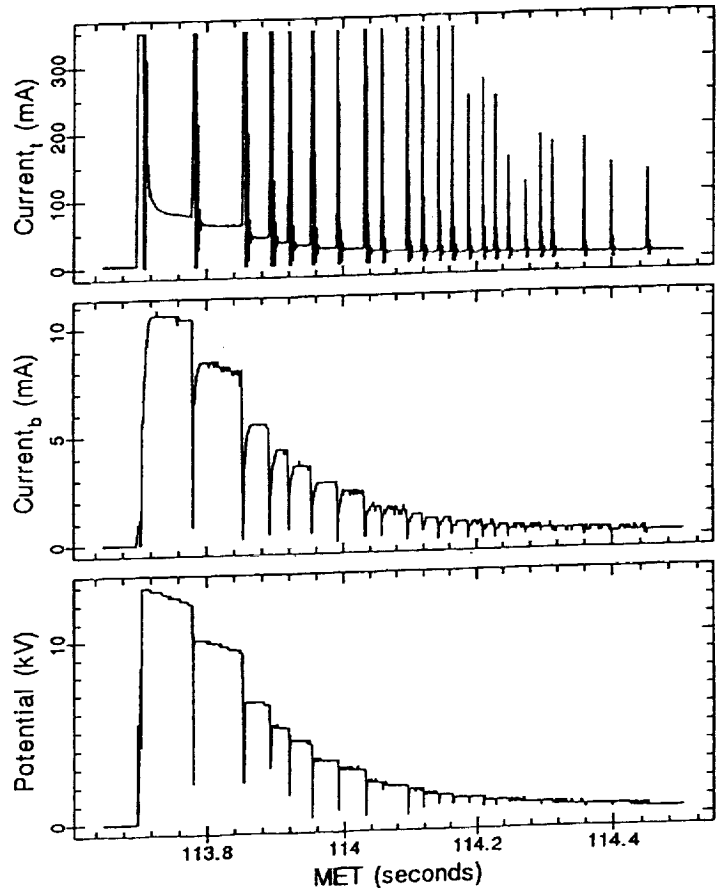


Fig. 10. The measured boom and total current, and the potential on sphere 1 versus time during the vacuum plasma chamber tests.

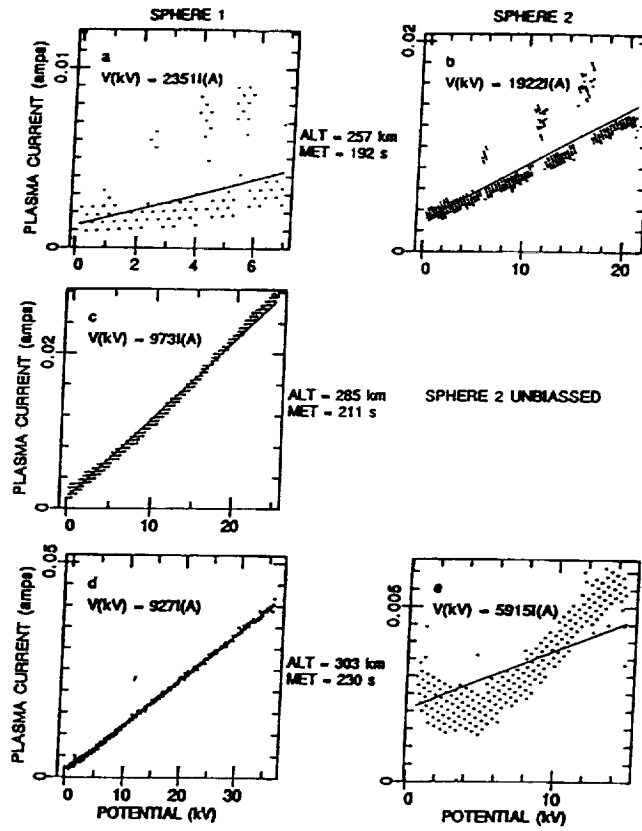


Fig. 11. Plasma current versus voltage for both spheres during the first three voltage bias operations of the experiment.

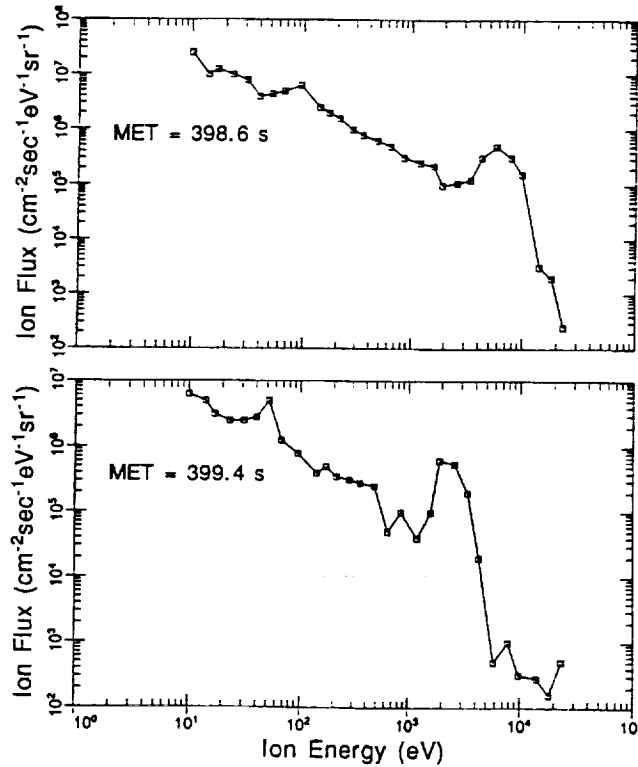


Fig. 12. The ion flux data versus energy for two sweeps of the particle detector during one voltage bias operation at 361 km.

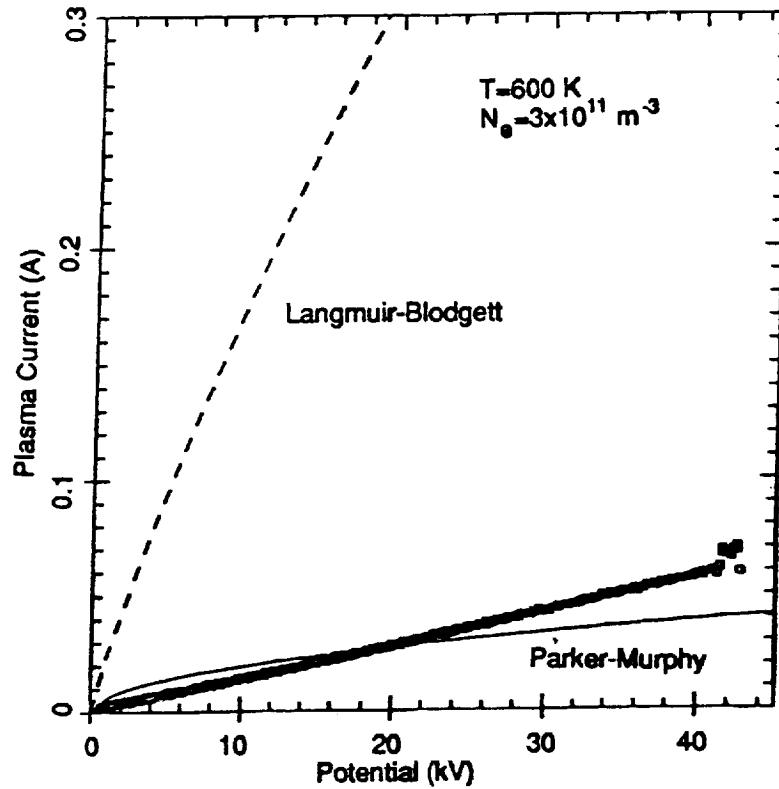


Fig. 13. The plasma current versus potential of sphere 1 at 361 km. The Langmuir-Blodgett and Parker-Murphy models are shown for reference.

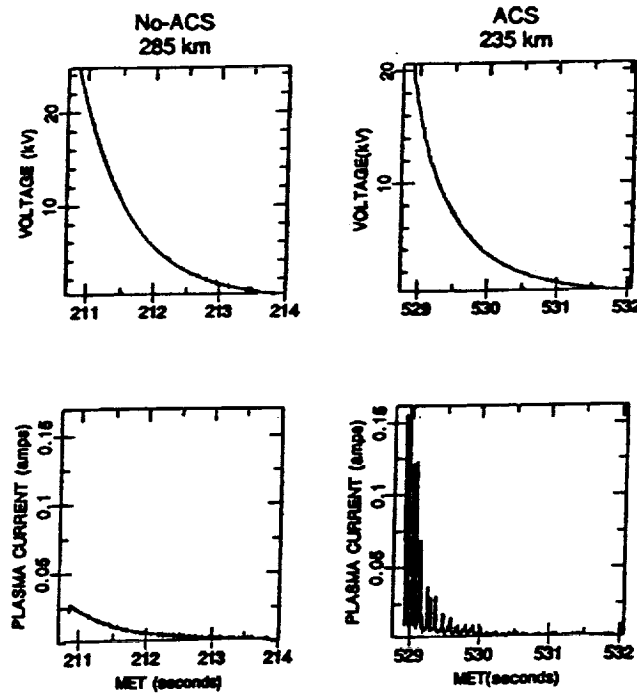


Fig. 14. The voltage (top panels) and plasma current (bottom panels) for voltage bias operations without ACS activity at 285 km (left panels) and during ACS activity at 235 km (right panels).

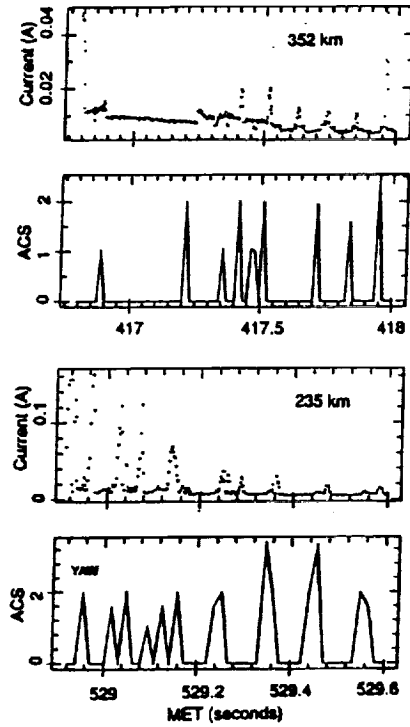


Fig. 15. Enhancement of plasma current correlated with ACS nozzle firings at 352 km (top two panels) and 235 km (bottom two panels).

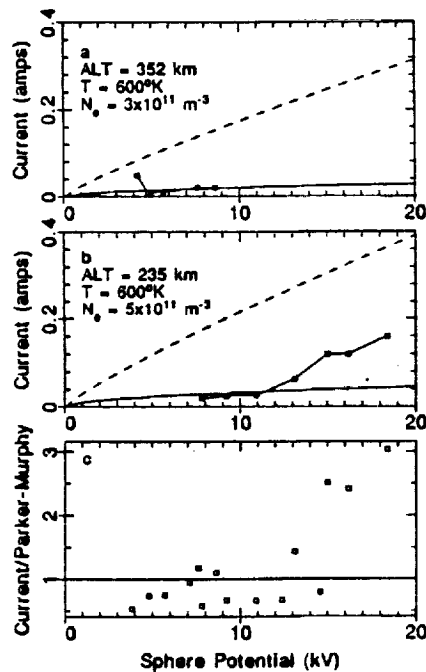


Fig. 16. Plasma current to the sphere versus sphere-to-ionosphere potential (top two panels) measured when ACS activity reduced the rocket body potential. The lower panel shows the sphere current normalized to the Parker-Murphy model versus sphere potential for all operations when the ACS reduced the rocket body potential. The numbers next to data points indicate the bias operation number where different from the top two panels.

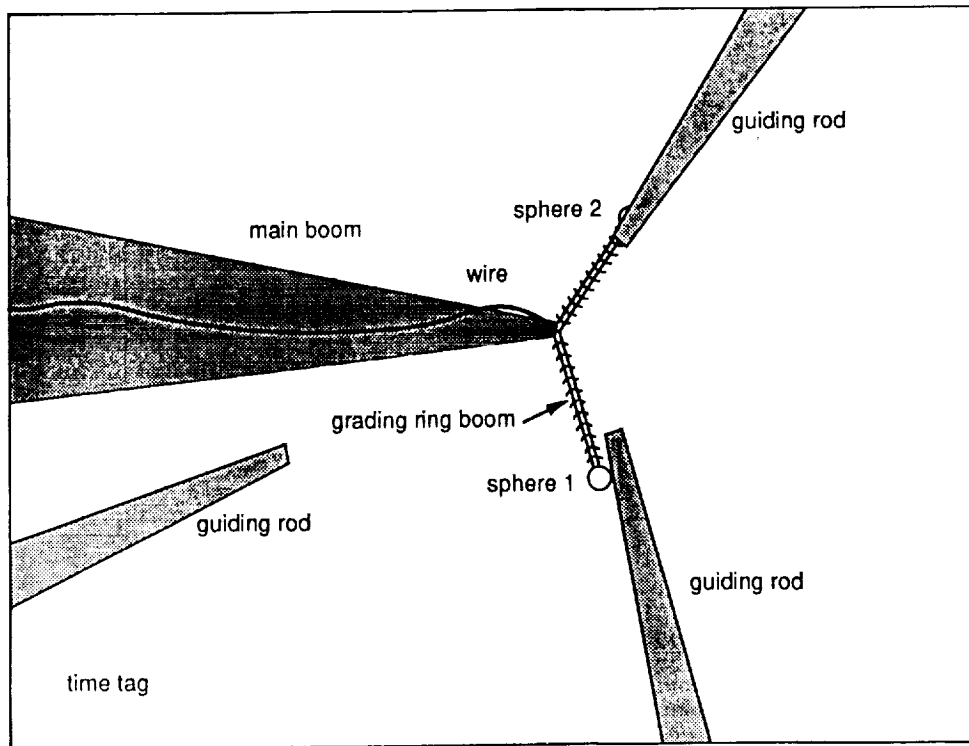


Fig. 17. Schematic representation of the view from the LLLTV camera.

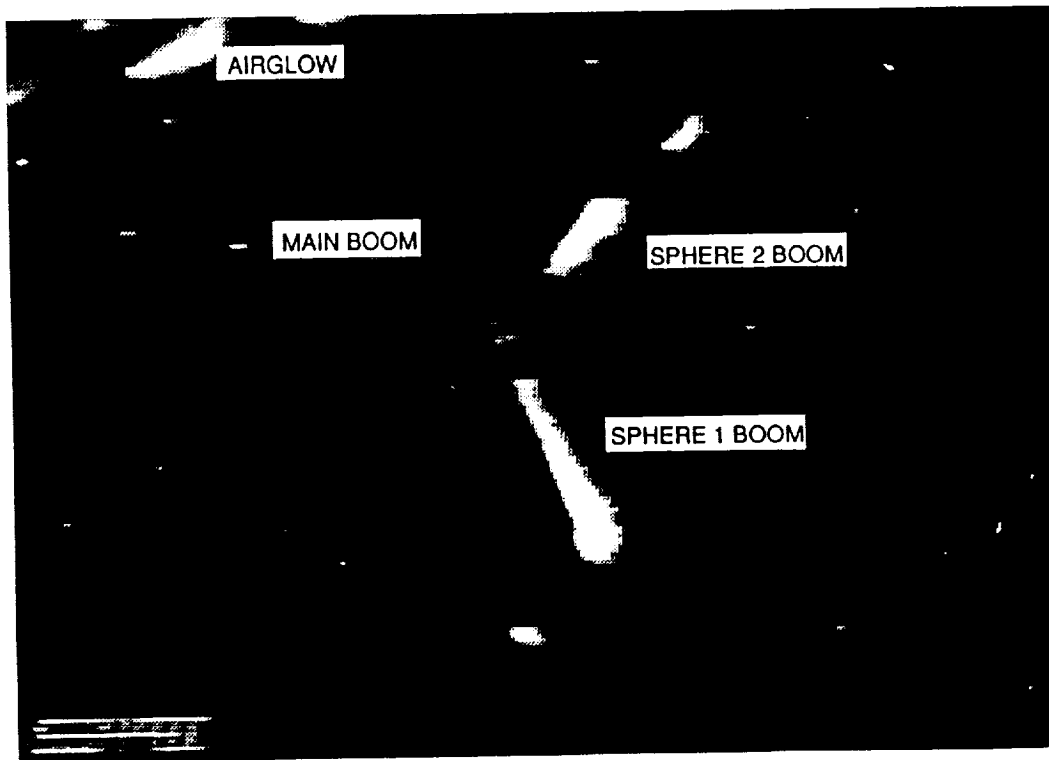


Fig. 18. Image from the LLLTV during a typical voltage bias operation at 235 km. Maximum voltages of 7 kV for sphere 1 and 21 kV for sphere 2 were applied.

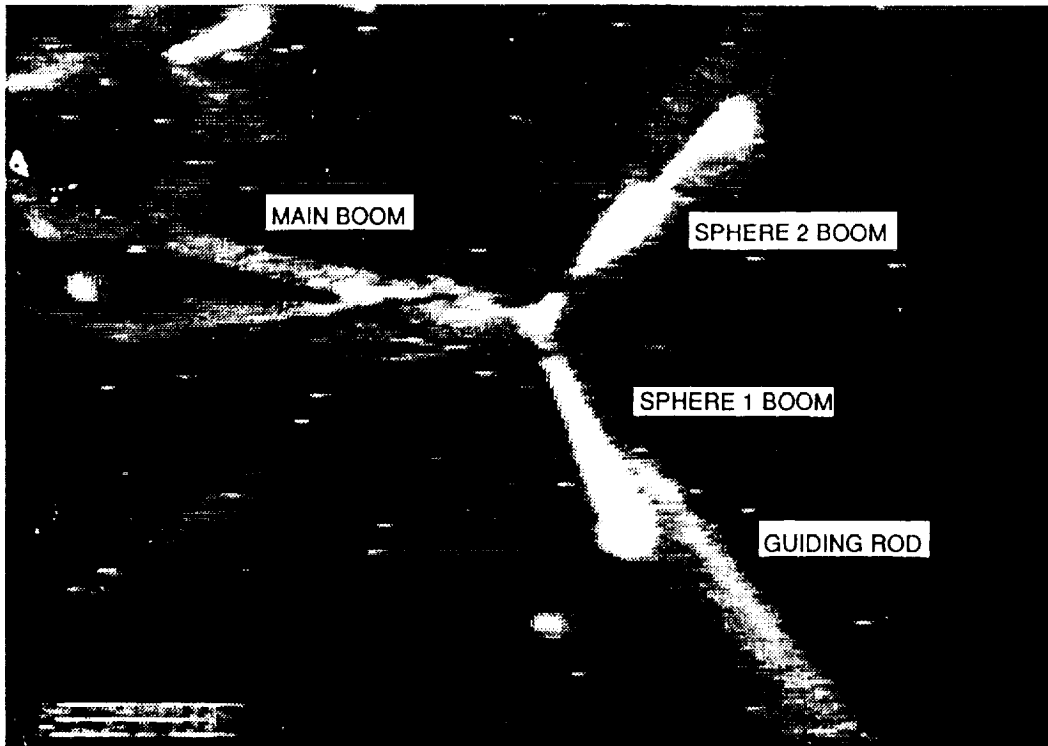


Fig. 19. Image from the LLLTV for the same voltage bias operation as Figure 18 just after an ACS gas release.

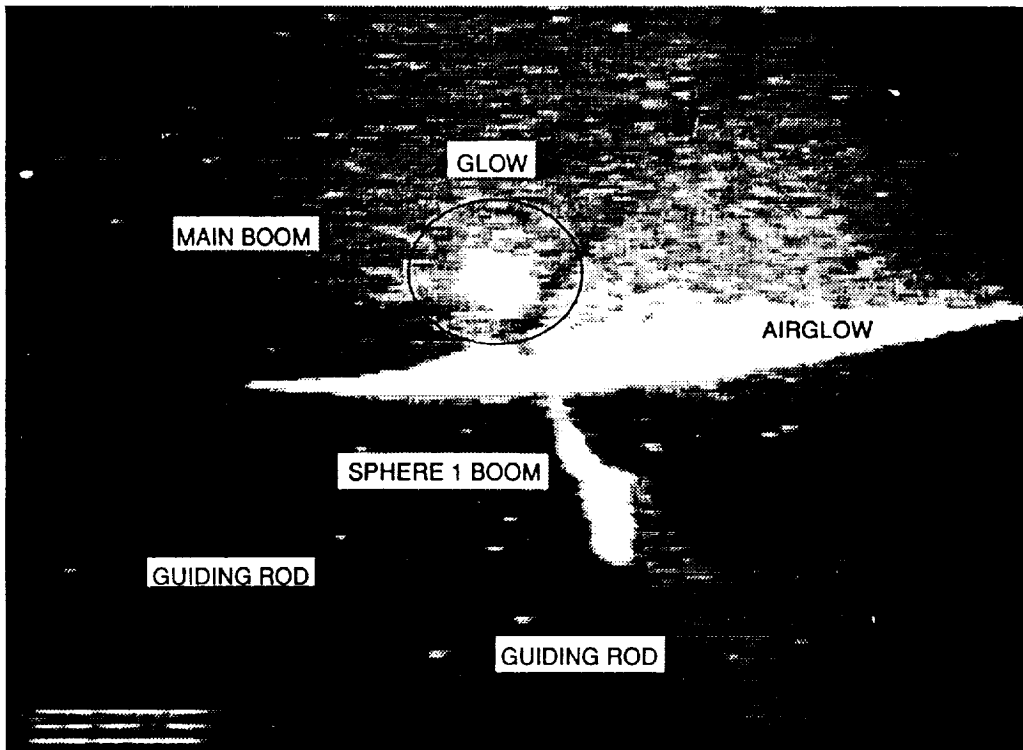


Fig. 20. Image from the LLLTV for a sphere 1 potential of 43 kV at 263 km.